Pergamon

Int. J. Solids Structures Vol. 35, No. 36, pp. 5097–5113, 1998

Printed in Great Britain
0020–7683/98/$—see front matter

PII: S0020–7683(97)00209–6

SPHERICAL INDENTATION OF COMPOSITE LAMINATES WITH CONTROLLED GRADIENTS IN ELASTIC ANISOTROPY

O. JØRGENSEN,†‡ A. E. GIANNAKOPOULOS† and S. SURESH*†

† Department of Materials Science and Engineering, Massachusetts Institute of Technology, Cambridge MA 02139, U.S.A.; ‡ Materials Department, Risø National Laboratory, DK-4000, Roskilde, Denmark

(*Received* 23 *November* 1996; *in revised form* 25 *June* 1997)

Abstract—Three-dimensional elastic analyses and experiments of indentation of thick laminated plates of carbon fiber reinforced epoxy are presented. Pointwise, the material is characterized as a linear elastic orthotropic material. The in-plane orientation of the carbon fibers is systematically varied as a function of depth. The influence of fiber orientation as a function of depth on the indentation response is considered along with the relationship between the indenter force vs depth. The fiber orientation profiles considered are those of a continuous linear variation between 90° at the outer surfaces and 0° at the center plane of the laminate, and a cross ply laminate involving alternating 90° and 0° layers through thickness. Experimentally, it is found that for the case of a cross-ply laminate, the indentation produces delaminations localized at the interfaces that separate planes of dissimilar orientation. For this case, stress concentrations at interfaces between plies of dissimilar orientation coincide with the observed sites of delamination. For the graded case, evidence of enhanced nonlinear deformation is found, without the nucleation of cracks. Computations show that for the graded material, tensile stresses perpendicular to fibers are suppressed significantly, possibly explaining the absence of matrix cracks in this material. Measured and computed indenter force-depth variations were found to be in good agreement. Experiments and computations also reveal that the orientation-graded material is more compliant when subjected to indentation than the conventional cross-ply laminate.

1. INTRODUCTION

Fibers of high strength and stiffness are widely used in lightweight structures. Continuous fibers embedded in a polymer matrix, commonly referred to as a lamina or ply, form the building blocks of laminated composites. Such composite panels can be tailored to meet various in-plane stiffness or strength requirements by appropriately stacking together similar orthotropic plies of dissimilar orientations. Similar arrangements have been analyzed extensively within the context of classical beam and plate theory. By contrast, comprehensive design of laminates that carry highly concentrated loads perpendicular to their surfaces is rarely treated. Such type of loading, as exemplified by indentation, impact, or other types of contact, cause stress concentrations at interfaces between ply groups of dissimilar anisotropic orientation. These stress concentrations are generally responsible for the susceptibility of these materials to transverse loading. In the case of spherical indentation of cross-ply laminates, such stress concentrations are known to initiate transverse cracks and delaminations, Jørgensen (1994a). Transverse cracks or splitting of fibers in combination with extensive delamination, lower the indentation strength and eventually allow the penetration of the indenter. This particular failure mode is a key concern in many applications.

The purpose of this paper is to propose a rationale for designing laminates which suppress failure by indentation. The material system we focus attention on is constructed by many thin laminae of fiber reinforced polymers stacked to form a thick laminated plate specimen. Within each layer, the material is characterized as orthotropic. One aim of this work is to demonstrate that, by choosing a functional dependence of the orientation of the fiber axes through the thickness of the plate, the indentation strength can be improved drastically. For this purpose, we compare a discontinuous orientation distribution, as

* Author to whom correspondence should be addressed.

exemplified by a cross-ply laminate, with specimen containing continuously graded variations of the fiber orientations through the thickness. The latter concept is believed to be new to the composites community and, as shown later, it arises from consideration of the stress fields under indentation in laminated elastic composites.†

Following prior work on discontinuously arranged cross-ply laminates, we assume that failure caused by the spherical indentation is initiated by tensile stresses perpendicular to fibers, Jørgensen (1994a). The transverse tensile strength of a typical fiber reinforced epoxy, containing a volume fraction of fibers of 50–65%, is in the range 10^1–10^2 MPa, whereas the tensile strength in the longitudinal direction is in the range 10^3 MPa. Considering these strength characteristics, it is desirable to choose a lay up configuration which minimizes tension perpendicular to fibers. The magnitude and sign of the projection of the stresses onto the material coordinate system therefore becomes a major issue. In fact, the issue of how the fibers shall be loaded so as to avoid damaging the matrix, albeit critical, appears to have been largely overlooked in most works on indentation and impact of composite materials. The reason for this is primarily that little is known about the distribution of stresses in inhomogeneous anisotropic media subjected to indentation, because of the difficulties in solving the relevant elasticity problems.

Willis (1966) considered the general Hertz problem for anisotropic bodies and determined the area of contact, as well as the pressure distribution of the contacting bodies. He showed that the contact area of a half-space with a rigid sphere is an ellipse, and that the pressure distribution is semi-ellipsoidal. Dahan and Zarka (1977) presented the analytical solution for the stresses of an elastic contact between a sphere and a semi-infinite transversely isotropic body. They found closed-form solutions for stresses along the axis of the punch and on the indented surfaces. Gibson and Kalsi (1974) analyzed the surface settlement of a linearly inhomogeneous, transversely-anisotropic elastic layer. Gibson and Sills (1975) examined the plane strip load problem of a linearly orthotropic incompressible elastic half space.

For the elastic indentation of a layered orthotropic body involving many layers of different orientation, only a full three-dimensional (3-D) analysis will suffice. As no known analytical methods exists for the problem considered here, we rely on the finite element method. For apparent computational reasons, the conventional 3-D analysis becomes exhaustive when considering many layers of different orientation. For example, in order to capture the field variations, including stress concentrations at interfaces, a fine resolution involving many 3-D elements through thickness is required. The method developed by Jørgensen (1993) has previously proven capable of meeting this particular requirement.

Indentation of an anisotropic material with a through-thickness gradient in in-plane material orientation has, to the best of our knowledge, never been treated. There do, however, exist analytical and numerical studies on elastic indentation of isotropic materials with through-thickness gradients in Young's modulus, Giannakopoulos and Suresh (1997a,b). These studies show, that for Young's modulus increasing monotonically and convexly with depth, the tensile stresses in the radial axial plane are generally lowered. In some cases, a functional dependence of Young's modulus can be prescribed in relation to the Poisson ratio, which causes the components of stress to be compressive through the entire body. This may be of importance to the failure of these materials, since the radial/axial tension is believed to cause the formation of cone cracks which are typically found in brittle materials subjected to Hertzian indentation. In the case of a decreasing Young's modulus with depth, enhanced tension results near the surface. Given this background information, we seek here to investigate the layering of orthotropic materials with a prescribed continuous and monotonous functional dependence of the material orientation through the thickness.

2. THE ANALYSIS OF THE ANISOTROPIC CASE

The elastic anisotropy of polymers reinforced with aligned continuous fibers is very well described by orthotropic constitutive material laws, e.g., Jones (1975). In our case, the

† O. Jørgensen, A. E. Giannakopoulos and S. Suresh, "Layered Composite Construction Including Controlled Mechanical Property Gradient Resistant to Indentation", MIT Case No. 7705, U.S. Patent Application filed June, 1997.

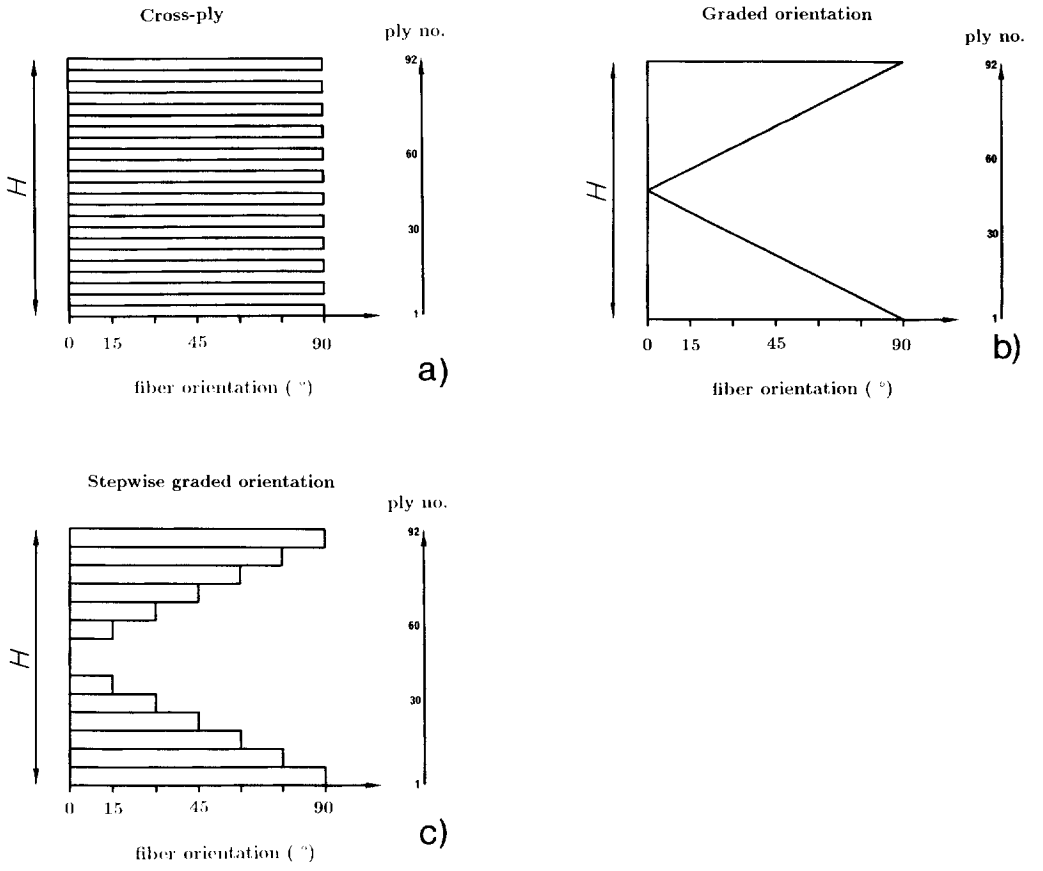

Fig. 1. Lay-up configurations. (a) Cross-ply material; alternating 0 and 90° layers. (b) Linear distribution of fiber orientation. (c) Stepwise linear distribution of fiber orientation.

model material is an epoxy reinforced with carbon fibers. The elastic constants for this material can be determined from measured natural frequencies of plate specimens with free boundaries, Frederiksen (1995). Hence, as far as linear elasticity is concerned, the constitutive relation between stresses and strains in the base material (i.e. the sublayers of the laminate which is made up of the unidirectional fiber-reinforced epoxy) is considered known. But deriving the distributions of loads in the various lay-up configurations subjected to indentation requires the solution of three-dimensional field equations. The lay-up configurations that we will consider are those of a symmetric cross-ply laminate comprising 0° and 90° fiber direction layers and that of a continuous linear or stepwise variation of fiber orientation through thickness. The latter has fibers oriented in 0° at the bottommost and topmost surfaces and 90° at the center of the specimen. The cross-ply laminate comprises 23 alternating 0° and 90° layers of equal thickness, Fig. 1(a). It is symmetric with respect to the midplane, i.e. the center plane of the 12th layer. The overall thickness, H, of the laminate at 12.6 mm. The linear case comprises a continuous linear change of the fiber orientation from 90° at the topmost surface to 0° at the center plane, Fig. 1(b). The center plane is a plane of symmetry of the plate. The overall thickness of the plate is 12.6 mm. It can be argued that a true linear variation, as treated above, can hardly be obtained in reality. Changes in material orientation will inherently be stepwise due to any layering process. In order to simulate this realistic case, we approximate the linear variation with a corresponding stepwise one, Fig. 1(c); here the fiber orientation changes by 15° in each step.

Relating observations of indentation failure to predicted stress fields requires a combined numerical and experimental effort. For this purpose, we use a symmetric double indentation test wherein indentation of two specimens arranged on top of each other is

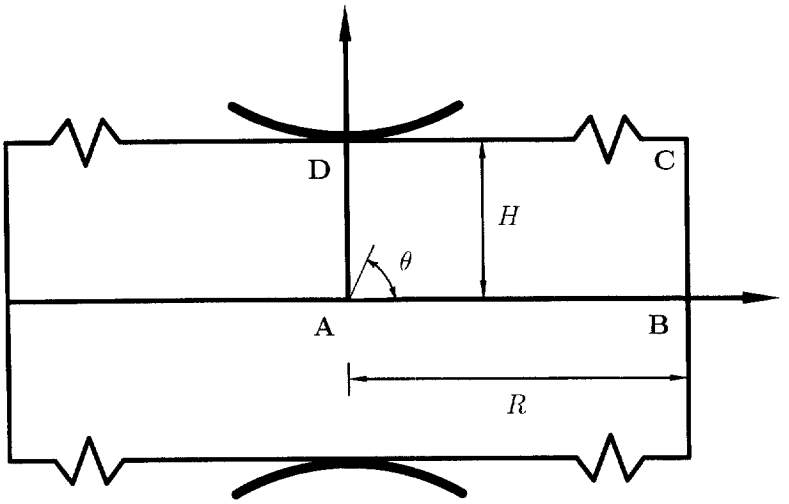

Fig. 2. Double indentation. The two specimens are positioned between the two spherical indenters. The plane of contact separating the two laminates is a plane of mirror symmetry.

Table 1. Elastic properties used in the modeling of the CFRP material

E_L	E_T	G_{LT}	ν_{LT}	ν_{TT}
(GPa)	(GPa)	(GPa)		
120	7.7	3.72	0.33	0.45

performed as depicted in Fig. 2. In subsequent analysis, (r, z) denote the axisymmetric polar coordinates, see Fig. 2, with a corresponding displacement (u, w). The circumferential direction is denoted by θ with the corresponding displacement v. The center plane, marked A–B in Fig. 2, is a plane of symmetry. Note that the origin of the (r, z) coordinate system is located at the intersection between the loading axis, marked D–A in Fig. 2, and the horizontal plane of symmetry. This setup allows for the indentation of thick plates without bending or free edge surface boundary effects, provided that the free boundary is remote from the point of indentation. The characteristic length-scales relevant to the problem are:[1] the diameter of the indenting sphere, D, overall thickness of the laminate, H, and the radius of contact, a. Also, the through thickness inhomogeniety implies a length scale. In the case of a layered composite, it is the thickness sequence of individual plygroups, h_n, whereas in the case of a graded composite, it is the change in orientation per unit depth. It is understood that, for continuum analyses to be valid, all of the above lengths should be at least an order of magnitude larger than the fiber diameter (approximately 7 μm).

Constitutively, the material of an individual layer can then be considered to be a homogeneous orthotropic material with special transverse isotropy. Note that here transverse isotropy means that the material is isotropic within a cross section which is perpendicular to the fibers. This means that the linear elastic behavior of each layer is established through five independent material constants, namely Young's modulus along the fiber axis E_L, the normalized transverse modulus E_T/E_L, the normalized shear modulus G_{LT}/R_L and two Poissons ratios ν_{LT} and ν_{TT}. ν_{TT} denotes the Poisson ratio with the transverse isotropic plane and ν_{LT} is defined as the relative transverse contraction strain when subject to uniaxial tension in the fiber direction. Within the context of an elasticity formulation, these five constants completely characterize the material response irrespectively of the particular combination of material and fiber material choice or fiber content. The material data used for the analysis is given in Table 1.

[1] Conway and Engell (1968) showed that the influence of the laminate thickness, H, on the force–depth relation and the stress fields is small, if $H > 5a$. It will be shown that this is the case for the present case.

A systematic study of the parametric variation of all the parameters of the problem is beyond the scope of this work. Therefore, we undertake the general numerical methodology in an attempt to extract a physical basis for interpreting experimental findings on real materials. Consequently, all length scales and properties are chosen to match, to the extent possible, those of the experiments reported in Section 3.

2.1. *Finite element formulation of the elasticity problem*

The modeling aspects of the double indentation problem are outlined in the following. Owing to the symmetry about the midplane of the test, Fig. 2, only the upper plate specimen is considered. We make use of the ring finite element developed by Jørgensen (1993). The ring-element concept applies to finite elements which are bodies of revolution. Hence, upon using a ring element, the modeling is restricted to specimen geometries which show rotational symmetry. This is, however, not a limitation here, since only situations independent of the outer boundary of the plate are of interest. The material that forms the body does not show rotational symmetry. Indeed, the material shows a strong directional dependence within the plane of the plate or ply. The directional dependence, in addition to the symmetries which define orthotropy, do, however, show π-periodicity. By this we mean that the elastic characteristics of the material are invariant in any rotation, θ, which is a multiple of π. Provided that the boundary conditions preserve this periodicity, the resulting displacement field will be π-periodic as well. This means that the appropriate displacements can be Fourier-expanded in terms of π-periodic harmonics without any loss of generality, Jørgensen (1993). The displacement field variables are preferably expressed with reference to a cylindrical coordinate system. Let u, v and w denote the radial, circumferential and the axial component of the displacements, respectively.

$$u(r,z,\theta) = \sum_{n=0}^{N} u_n^c(r,z)\cos(2n\theta) + \sum_{n=1}^{N} u_n^s(r,z)\sin(2n\theta) \tag{1}$$

$$v(r,z,\theta) = \sum_{n=0}^{N} v_n^c(r,z)\cos(2n\theta) + \sum_{n=1}^{N} v_n^s(r,z)\sin(2n\theta) \tag{2}$$

$$w(r,z,\theta) = \sum_{n=0}^{N} w_n^c(r,z)\cos(2n\theta) + \sum_{n=1}^{N} w_n^s(r,z)\sin(2n\theta) \tag{3}$$

The superscripts c and s denote the corresponding amplitudes in the cos and sin terms of the above Fourier expansions of the displacements. In the present case the absence of any stress singularity makes the above expansion complete. Equations (1)–(3) characterize the entire field to a radial/axial (r,z) plane of reference. The benefit of this method is the high rate of convergence of the above series. The significance of the truncation number, N, is important. Note that $N = 0$ corresponds to the limiting case of an axisymmetric deformation. The displacement boundary conditions along the center axis are:

$$\lim_{r\to 0}(u) = 0, \quad \lim_{r\to 0}(v) = 0, \quad \lim_{r\to 0}(w) = w(z) \tag{4}$$

which in view of eqns (1)–(3) transform to

$$n \geqslant 0: \quad u_n^c(0,z) = v_n^c(0,z) = u_n^s(0,z) = v_n^s(0,z) = 0, \quad n \geqslant 1: \quad w_n^c(0,z) = w_n^s(0,z) = 0 \tag{5}$$

Along the center plane of the test, $z = 0$, the symmetry condition is invoked. The condition of symmetry is $w = 0$, which in combination with eqns (1)–(3) gives

$$n \geqslant 0: \quad w_n^c(r,0) = w_n^s(r,0) = 0 \tag{6}$$

At the outer boundaries $r = R$, where R is the radius of the circular plate, and $z = 0$, which is the uppermost surface, stress-free boundary conditions are imposed. It is known from Conway and Engell (1968) that for $R \gg 7a$, the influence of the outer boundary, i.e. R, essentially becomes insignificant to the problem.

Linear kinematics, linear elasticity and small strains are assumed. Within the radial/axial plane of reference, the field variables, u_n^c, v_n^c, w_n^c, u_n^s, v_n^s, w_n^s, are resolved in terms of eight-noded isoparametric finite elements. Note that the number of degrees of freedom per node depends on the choice of N. For a given N, the stiffness matrix of each ring-element is integrated. The integration with respect to the circumferential direction involves products of harmonical functions of θ. This is due to the displacement assumption, according to which displacements are expanded in the Fourier series, eqns (1)–(3), and also due to directional dependence of the stress strain relation, see Jones (1975). It is important to note, that the integration with respect to the circumferential direction is performed analytically. The details of this specific part of the integration procedure are given in Jørgensen (1993). Numerical integration of the element is applied in the radial axial plane. The choice of an eight-noded isoparametric element allows a continuous variation of the material orientation across the element. That is, at each integration point the material is oriented according to the depth/orientation relation. A typical mesh is depicted in Fig. 3. It consists of 1500 elements and 4661 nodes. Truncation of the expansions eqns (1)–(3) by $N = 4$, implies that the model comprises a total of 121,186 degrees of freedom. The convergence of the series was checked by varying the truncation number, $N = 1, 2, 3, 4, 5$. It was found that $N = 2$ produced very good approximations and that $N = 4$ can be considered sufficient for the convergence of the circumferential field variations in the analysis reported here.

The indenter is a rigid sphere which indents the center of the top surface ($r = 0$, $z = H$) in the model. The contact is considered frictionless throughout the analysis. Nodal contact is considered for 11 nodes comprising the topmost surfaces of five elements. The solution of the contact is established through an incremental procedure. That is, the indenter is displaced in increments and at each increment the displacement solution is established. The size of each increment, δ, is chosen so that for all contact nodes $\delta \ll 2r_i(r_{i+1} - r_i)/D$, where r_i is the radial position of the ith node in contact. Obviously, the node positioned on the axis of indentation makes contact during the very first increment. Hence, the vertical displacement of this node exactly equals the displacement of the indenter. Nodes at increasing radii make contact successively. A node can achieve contact along the entire circumference or along parts of it. If the node has achieved contact along the entire circumference, then the vertical displacement increments are identical to the increments of the indenter. If a node is only partly in contact, then the vertical displacement increment of this node is prescribed in the angular region where contact is achieved. This means that the Fourier coefficients of eqn (3) and a Fourier expansion of the displacement increment to

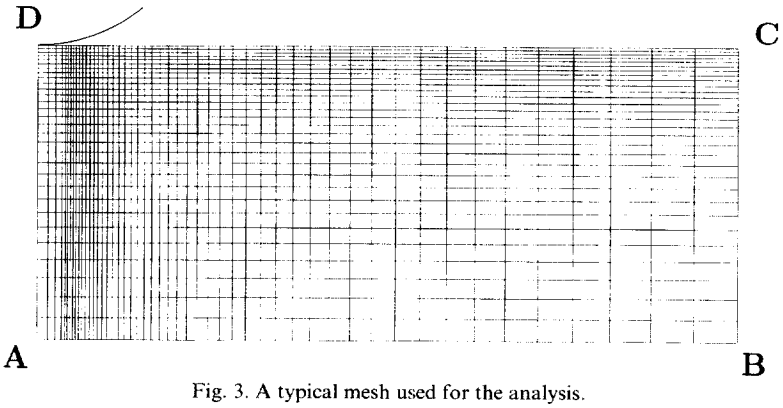

Fig. 3. A typical mesh used for the analysis.

be prescribed accordingly. In our case, this expansion is performed numerically by means of a set of standard Fast Fourier Transform (FFT) routines, Press *et al.* (1989). Since a node can be partly in contact, the Hertzian contact perimeter for anisotropic bodies is not in general circular, Willis (1966). In all the cases considered in this work, it was found that the contact node at the perimeter of the contact area was initially in contact only partially. Contact along the entire perimeter was achieved upon further loading. Naturally, this effect depends on the truncation number, N, and the mesh. However, it is seen, that the contact pressure drops to zero at the contact perimeter. Hence, the inaccuracy of predicting the exact shape of the boundary of the contact area is believed only to have a second order effect on the force-depth prediction and on the predicted stress fields.

2.2. *Numerical results*

Since strength and failure are important issues in indentation, we will focus on tensile stresses perpendicular to fibers. This particular projection of stresses is mapped onto the plane of reference, ABDC in Fig. 2. That is, at each point of the plane of reference ($\theta = 0°$) we will plot the maximum tensile stress perpendicular to fibers for any angle, θ, between 0 and π.

2.2.1. *The cross-ply case.* The material texture of the cross-ply laminate is depicted in Fig. 1(a). The distribution of maximum tensile stresses perpendicular to fibers, corresponding to an overall indenter force of 5000 N, is depicted in Fig. 4. Clearly stress concentrations are present at the interfaces between layers of dissimilar orientation.[2] The highest level of tension is found in the uppermost interface. Stress concentrations are located in the layers below as well. Note that the stress amplitude decreases markedly with depth. In the upper two interfaces the tensile stress perpendicular to fibers exceeds the strength of the material, which is approximately 80 MPa transverse to fibers; hence, failure is expected at these sites. The material points being subjected to the highest tensile stress perpendicular to fibers consistently occur in the half-plane $\theta = \pi/2$ for the 0° layers and in the half-plane $\theta = 0°$ for the 90° layers. These half-planes define the quarterplate symmetry which is evident for the cross-ply geometry. The maximum tensile stresses, as well as the maximum compressive stresses, within these planes are principal stresses due to this quarter model symmetry. The maximum tension perpendicular to fibers occurs in the transverse planes of symmetry. The tensile stresses are therefore on the principal plane.[3]

2.2.2. *The linear variation case.* The texture of the material with the linear variation is depicted in Fig. 1(b). The load was applied incrementally, reaching a maximum of 5000 N. The distribution of maximum tensile stresses perpendicular to fibers corresponding to this load level is depicted in Fig. 5(a). Note that projecting the maximum tensile stress perpendicularly to the fibers onto the (r, z) plane facilitates the visualization of the stress amplitudes through the thickness of material. The tensile stresses plotted in Fig. 5(a) are not principal stresses in general. The tensile stresses diffuse from the contact surface into the solid without reaching critical levels. This is in strong contrast to the stress concentrations present at the interfaces of the cross-ply laminate, Fig. 4. The corresponding angular positions of the material points being subjected to maximum tensile stress perpendicular to fibers are depicted in Fig. 5(b). That is the angular position relative to the material axis (local fiber direction) is given in degrees. Note that in the cross-ply case this relative angle was 90° throughout the body, corresponding to a tensile stress field perpendicular to fibers which is on one of the two principal planes ($\theta = 0°$ and $\theta = 90°$). Clearly the points of maximum tension perpendicular to fibers are not confined to any of the two specific radial planes. Also, the sharp distinction between tensile stresses being of the hoop type or the radial axial type is no longer obvious. For the graded material it is seen that a confined region around the axis near the indented surface is in compression.

[2] Such stress concentrations have been observed by Chen (1971) for the case of indentation of isotropic material with layers on a semi-infinite substrate, where each layer had a different elastic modulus. Jørgensen (1994a) numerically predicted stress concentrations in cross-ply laminated plate subjected to spherical indentation.

[3] The predicted elastic force–depth curve is given in Fig. 7.

Below this domain, the isostress curves define a zone of tensile stresses perpendicular to fibers relatively deep in the material and therefore with limited amplitude. From the surface, pointing into the material at an inclination of approximately 45° to the surface, a zone of tensile stress can be seen. The amplitude is moderate, below 50 MPa, and is therefore reckoned not to be critical. In the far field the angular position of the material points of maximum tension perpendicular to fibres are close to 0°. Note that positions below 0° (yellow zone in the far field) are here recognised in the interval 165°–180°. This is a consequence of the chosen scale in combination with the periodicity of the solution.[4]

2.2.3. *The stepwise linear variation.* The material texture is depicted in Fig. 1(c). The finite element mesh naturally has to reflect the stepwise layering. That is, element boundaries must meet the boundaries between materials of different orientation. The distribution of maximum tensile stresses perpendicular to fibers is depicted in Fig. 6. The stress fields clearly reveal an effect of the layering. However, the predicted field is close to that computed using the continuously graded assumption, Fig. 5(a). Note that this observation cannot be expected to hold for any contact radius or for any thickness of layers. In our particular case, the contact is achieved within a radius of 1.4 mm and the thickness of each layer or ply group is 0.9 mm. For the practical application and testing discussed in Section 4, we will consider contact radii above this value. Plies are of thickness 0.13–0.14 mm and the relative change in orientation between adjoining layers is 2°. This we will consider a good approximation to the graded idealisation.

3. EXPERIMENTAL METHOD

3.1. *Specimen preparation*

Two laminates were manufactured. One was a so-called cross ply laminate comprising 92 laminas grouped by four in 23 layers of alternating fiber direction 0 and 90°. The stacking sequence can be written as: $[90^\circ_4, 0^\circ_4, 90^\circ_4, 0^\circ_4, 90^\circ_4, 0^\circ_4, 90^\circ_4, 0^\circ_4, 90^\circ_4, 0^\circ_4, 90^\circ_4, 0^\circ_2,]_{SYM}$. The idealized conditions of a graded material orientation were approximated by use of plies arranged with a minimum of angular variation between neighboring layers. In the second case, 92 plies formed a laminate with a "graded" linear variation through thickness. The stacking sequence was: $[90^\circ, 88^\circ, 86^\circ, 84^\circ, \ldots, 6^\circ, 4^\circ, 2^\circ, 0^\circ]_{SYM}$. Essentially, the variation in orientation is stepwise, through the thickness. However, based on the findings of Sections 2.2.2 and 2.2.3, we expect this stepwise variation in orientation to be adequate. Both laminates were made from standard carbon fiber reinforced epoxy pre-pegs, denoted by the commercial name Sigrafil delivered by SIGRI, Germany. The overall thickness of the plates was 12.6 mm. Hence, in average each cured lamina was approximately 137 μm. Hence, the fiber volume fraction is lower in the present material than in cured plies of 125 μm thickness which is usually the standard for this material system. Measured values of the elastic constants are valid for plies of 125 μm thickness only. We have taken previously measured values and applied rules of mixture to obtain the values given in Table 1. From both plates square samples, 60×60 mm, were cut. The specimens were then gently ground on the top and bottom surfaces using 500 grade paper mounted on a water lubricated metallographic disc. This was in order to prepare co-planar surfaces for mounting in the double indentation fixture by removing excess epoxy from the surfaces.

3.2. *Testing*

Two specimens were placed on top of each other and mounted in the double indentation fixture, as shown schematically in Fig. 2. The specimens were oriented in order to preserve the midplane symmetry of the test. Indeed this is a prerequisite for the previous modeling to be correct. Load was applied using an Instron 8501 servohydraulic testing machine. The machine was operated under load control. Load was applied in all cases at a rate of 30 N/s. Three tests were conducted on each material. The final loads were 4000, 6000 and 10,000 N. The loading and unloading paths were recorded for all tests. After testing, the compliance

[4] The predicted force–depth curve is given in Fig. 7.

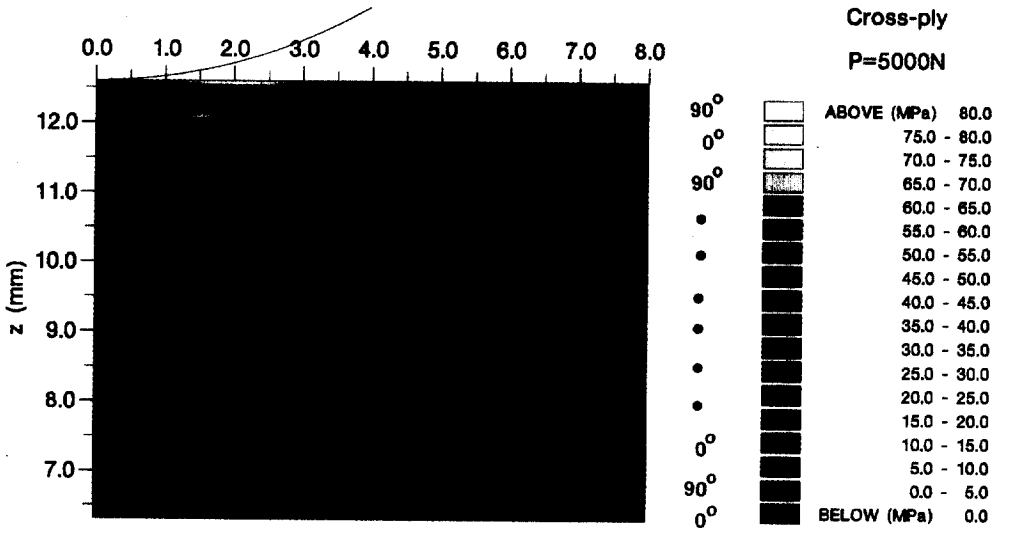

Fig. 4. Indentation induced stresses in the cross-ply material. Distribution of maximum tensile stresses perpendicular to fibers.

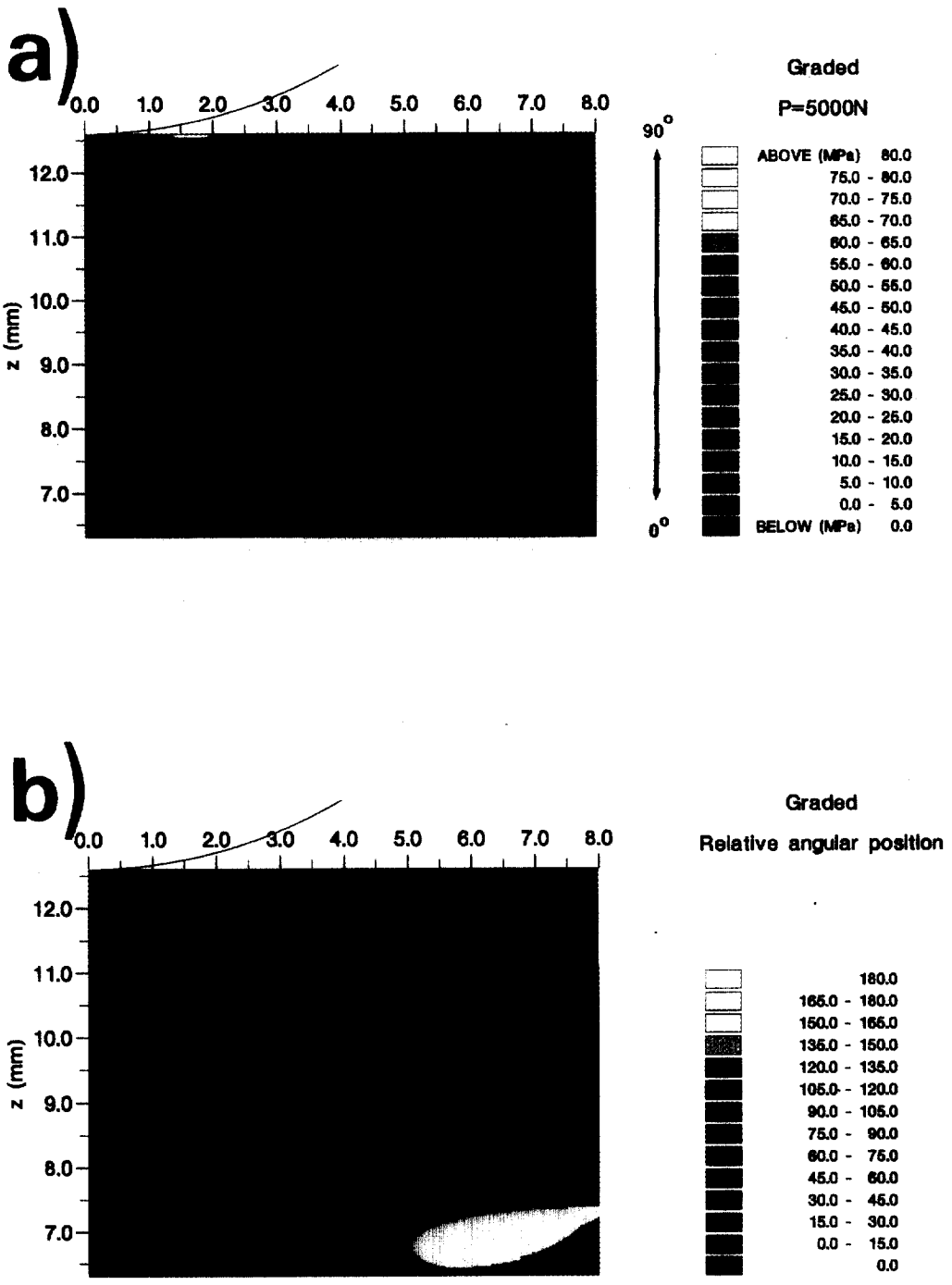

Fig. 5. Indentation induced stresses in the material with the linear fiber orientation distribution. (a) Distribution of maximum tensile stresses perpendicular to fibers. (b) Angular position of the material points being subjected to maximum tensile stress perpendicular to the fibers.

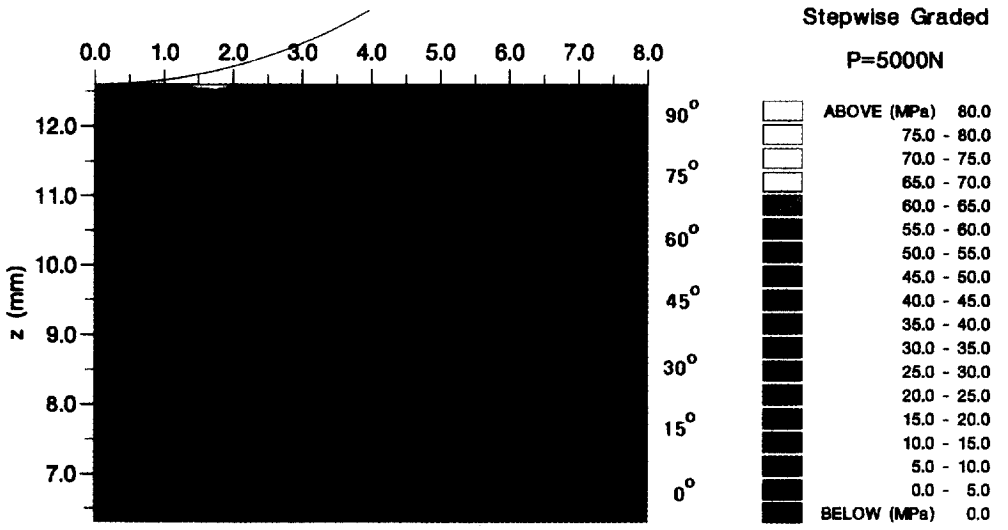

Fig. 6. Indentation induced stresses in the material with the stepwise linear fiber orientation distribution. Distribution of maximum tensile stresses perpendicular to fibers.

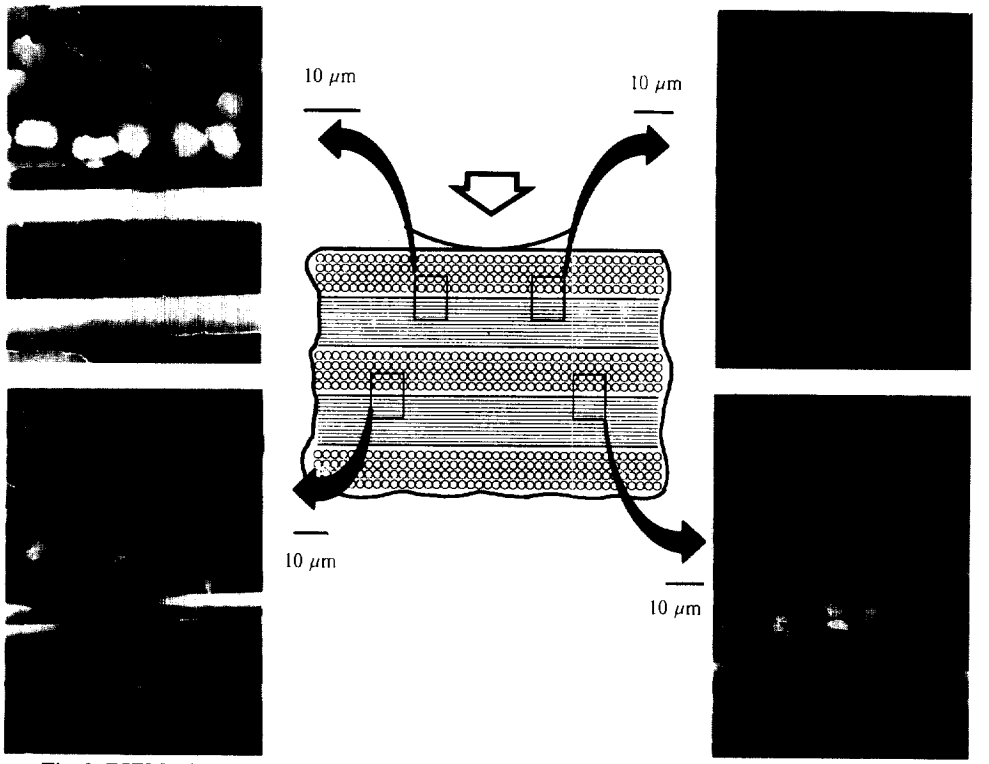

Fig. 8. ESEM micrographs showing interfacial microcracks in the crossply material at locations of tensile stress concentrations induced by spherical indentation.

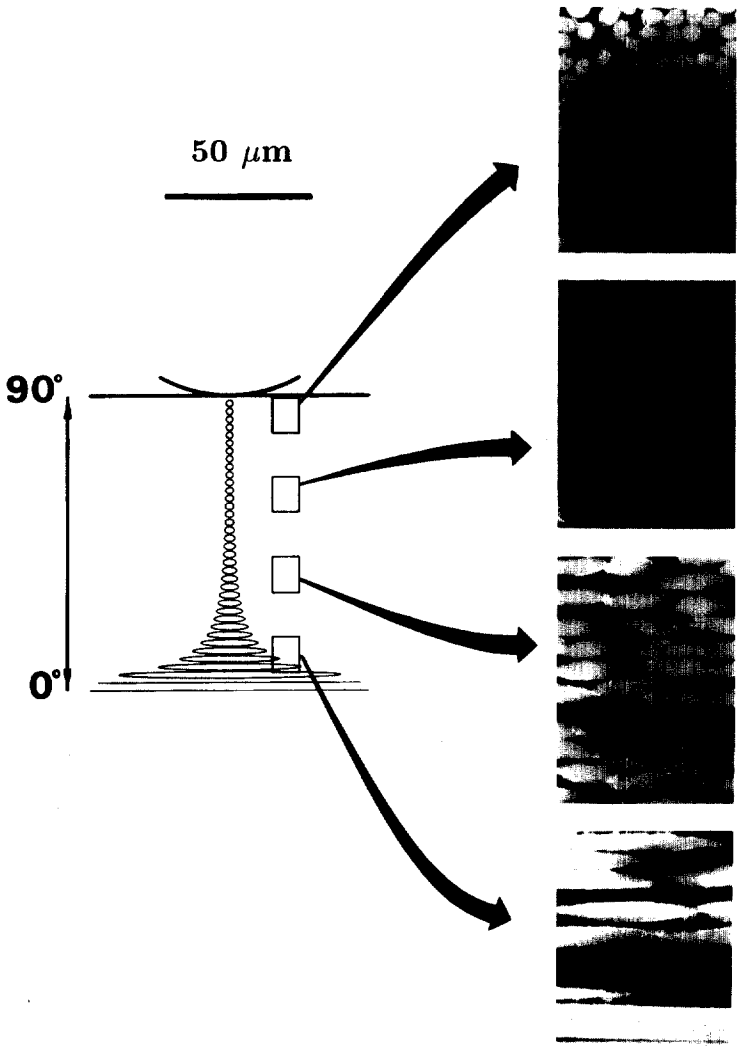

Fig. 9. ESEM micrographs of the material with the graded fiber orientation. No signs of failure are present. Note the cross sections of the fibers as they change from circular to elliptical with depth.

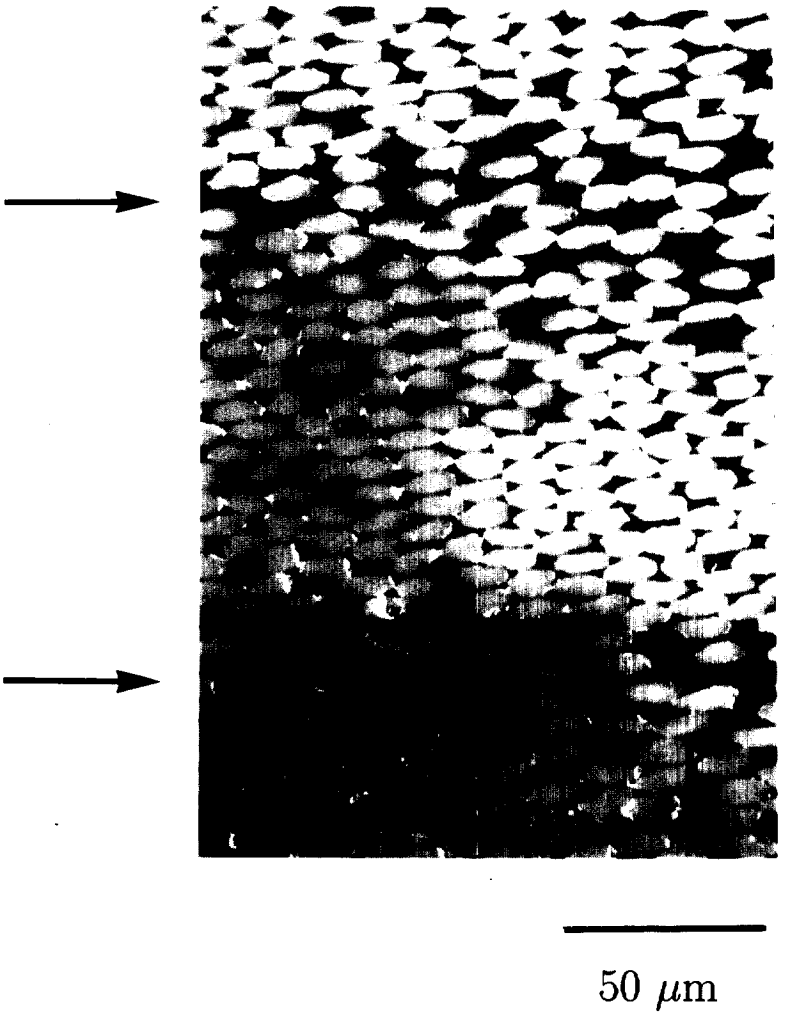

Fig. 10. ESEM micrograph of the material with the linearly graded fiber orientation. Horizontal zones of lower fiber density are found where the sheets of the ply material is assembled. There are no signs of stress induced failure within these zones.

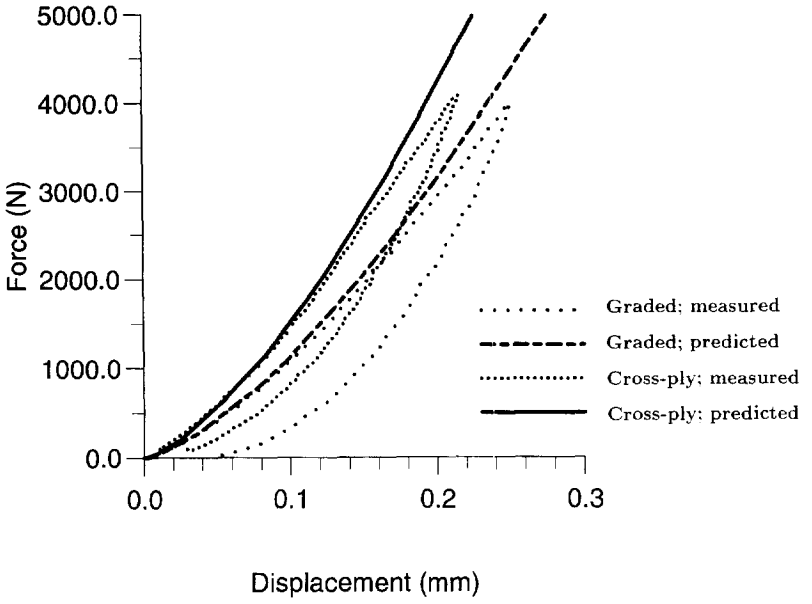

Fig. 7. Measured and predicted force–depth relations for the linearly graded orientation and the cross-ply material.

of the loading system was measured by applying force, while the two spherical indenters were in direct contact. The contribution to system compliance arises partly from elasticity of the entire loading machine, including load cell, bridge, etc. At sufficiently high loads this contribution is linear to a good approximation. The identation involves not only the indentation in the specimen, but also the loading fixture. The force–depth relation corresponding to this indentation is nonlinear. Provided that the contact is Hertzian, the force is proportional to $\tilde{w}^{3/2}$ where $\tilde{w}$ is the vertical movement of the crosshead corresponding to the overall compliance of the indentation testing rig. Hence the force–crosshead displacement relation takes the form:

$$\tilde{w} = \frac{P}{\tilde{A}} + \left(\frac{P}{\tilde{B}}\right)^{2/3} \tag{7}$$

Fitting data from the compliance test to the above expression resulted in the estimates $\tilde{A} = 125$ kN/mm and $\tilde{B} = 102$ kN/mm$^{3/2}$. In the force–depth curves to be given in the next paragraphs, we measured the vertical position of the crosshead and then subtracted the additional displacement, $\tilde{w}(P)$, to give the actual depth position of the spherical indenter from the surface of the tested material.

The tested specimens were sectioned and transverse sections were ground and polished with 1 μm diamond paste. The polished sections were investigated carefully using light microscopy, as well as scanning electron microscopy. The latter was performed in an Environmental Scanning Electron Microscopy (ESEM), fabricated by Electroscan. This type of electron microscope allows the observation of the specimen without charging the polymer.

4. COMPARISON BETWEEN EXPERIMENTS AND THEORY

The simulated and measured force–depth curves for the two laminated materials are plotted in Fig. 7. For both materials the predictions based on elastic analysis are close to the actual measured response for loading. The graded orientation results in a significant increase in compliance compared to the indentation of the cross-ply laminate. The increase in compliance, as well as the stress distribution and amplitude together suggest a relatively

more indentation resistant response, as compared to the cross-ply laminate. For both the graded and the cross-ply laminate, the predicted response is consistently stiffer than the measured. For the cross-ply laminate, however, a distinct loss in stiffness is found experimentally for the load of approximately 2800 N, where a kink in the measured force–depth response is seen. This kink is believed to arise from the onset of delamination. Above this load, the slope of the force–depth response is markedly softer than the predicted elastic response. The force-depth response for the graded material does not show a similar discontinuity in slope. The hysteresis of the graded material is, however, significant and even more pronounced than for the cross-ply laminate. Hence, the energy dissipation during the loading cycle is higher for the graded material than for the cross-ply laminate. The fact that the measured force–depth relation does not show any discontinuity in slope almost excludes the possibility of localized micro-delamination taking place during indentation. Delamination does involve a drop in shear stiffness of the structure, and will cause a softening in the force–displacement curve.[5] The absence of a discontinuity of the force–depth response renders that the hysteresis and dissipation of energy in the graded material is likely to be due to a deformation mechanism which is continuously distributed in the volume of material. Note also that contact friction can contribute to the measured response and that for fixed load, this contribution is expected to be higher for the graded material than for the cross-ply laminate, due to the larger contact area achieved in the former material. The interesting behavior of increasing compliance, as manifested in the force–depth curves, was also observed by Suresh *et al.* (1997) in isotropically graded materials. Suresh *et al.* (1997) also showed that the stress reduction due to decreasing elastic modulus with depth results in suppressing the indentation induced incipient plasticity. The present results are in line with these previous findings.

Figure 8 shows a scanning electron micrograph of a cross section of the tested cross-ply material. The exposed section is parallel to fibers in 90° layers and includes the axis of loading. The images reveal details of the failure pattern on either side of the axis of loading. The exposed material has been subjected to 6000 N indentation. At this load level, failure is expected in the 2–3 uppermost interfaces as per the analysis, Fig. 4. Microscopy reveals inclined cracks in the upper three interfaces, Fig. 8. The size of the cracks is of the order of a fiber diameter. The cracks show mirror symmetry with respect to the loading axis. The mirror symmetry applies to the position of the microcracked zone as well as the crack inclination.

It has not been possible to identify microfracture in the graded material, Fig. 9. Fraction of a cross section of the sample tested at 10 kN is shown in Fig. 9. Note the elliptic contour of each individual fiber as it changes with depth. Microscopy reveals the interfacial zones between plies as zones of relatively low fiber density, Fig. 10. These zones are spaced through the plate at a distance corresponding to the lamina size, i.e., approx. 140 μm. There are no signs in terms of cracking of this resin-rich region having been subjected to severe stresses.

5. CONCLUSIONS

Three-dimensional elastic analysis and experiments of indentation of thick laminated plates of carbon fiber reinforced epoxy have been performed. A detailed comparison between a layered anisotropic material and a graded one is carried out. The material orientation profiles considered are those of a continuous linear variation between 90° at the surfaces and 0° at the center plane of the laminate and a cross ply laminate involving alternating 0° and 90° layers through thickness. It is shown that grading the material orientation with depth implies a far more indentation tolerant material.

The graded orientation causes enhanced elastic compliance, as compared to the cross-ply case. This experimental finding is supported by detailed elasticity solutions, which show that the load-depth response is well predicted from an elastic analysis. For the cross-ply material, it was found that distinct stress concentrations exceed critical levels at interfaces

[5] Jørgensen and Horsewell (1997) predicted numerically and measured experimentally the softening arising from inserting elasto–plastic interleaves in cross-ply laminates.

between layers of alternating orientation. By contrast, stresses diffuse in the case of the graded material. Hence, for the same level of loading the stress amplitude is reduced below the critical level by a factor of 2. The loading paths of the indentation are well captured by the elasticity solutions. For the unloading, however, inelastic deformation is revealed in the form of hysteresis. For the graded case, evidence of enhanced hysteresis is found without this being associated with cracks. Scanning electron microscopy did not reveal any signs of microfailure of the graded material. By contrast, it is found that for the case of a cross-ply laminate, the indentation produces delaminations and microcracking localized at the interfaces which are separating plies of dissimilar orientation. This failure is located exactly where tensile stress concentrations are predicted numerically. The onset of failure causes a distinct softening which is detectable from the load-depth curve. The capacity of laminated composites to carry loads of the indentation and impact type is very much limited due to the loss of shear stiffness and strength following delamination. Indeed such type of delamination is associated with the structural collapse occurring during, for instance, penetration. Hence, whenever this particular failure mode is of interest to an application, fiber composites with a continuous variation in material orientation through thickness appears to be a good indentation resistant design.

Acknowledgements—The authors wish to thank C. Mikkelsen, A. Lystrup, G. Labonte and J. Alcala for their valuable help in this work. The work done by Ole Jørgensen at MIT was sponsored by the programme on layered structures within the Engineering Science Centre at Risø National Laboratory. A.E.G. and S.S. acknowledge support from the Office of Naval Research under Grant N-0014-93-1-1277 at MIT.

REFERENCES

Chen, W. T. (1971) Computation of stresses and displacements in a layered elastic medium. *International Journal of Engineering Science* **9,** 775–800.

Conway, H. D. and Engel, P. A. (1969) Contact stresses in slabs due to round rough indenters. *International Journal of Mechanical Sciences* **11,** 709–718.

Daham, M. and Zarka, J. (1977) Elastic contact between a sphere and a semi infinite transversely isotropic body. *International Journal of Solids and Structures* **13,** 229–238.

Frederiksen, P. S. (1995) Experimental procedure and results for the identification of elastic constants of thick orthotropic plates, DCAMM Report No. 506, Technical University of Denmark.

Giannakopoulos, A. E. and Suresh, S. (1997a) Indentation of solids with a gradient in elastic properties: Part I. Point force solution. *International Journal of Solids and Structures* **34,** 2357–2392.

Giannakopoulos, A. E. and Suresh, S. (1997b) Indentation of solids with a gradient in elastic properties: Part II. Axisymmetric indenters. *International Journal of Solids and Structures* **34,** 2393–2428.

Gibson, R. F. and Kalsi, G. S. (1974) The surface settlement of a linearly inhomogeneous cross anisotropic elastic layer. *ZAMP* **22,** 855–864.

Gibson, R. E. and Sills, G. C. (1975) Settlement of a strip load on a non-homogeneous orthotropic incompressible elastic half-space. *Quart. J. of Mech. and Math.* **28,** 233–243.

Hertz, H. (1882) Uber die beruhrung fester elastischer koper. *J. reine angewandte Mathematik* **92,** 156–171.

Jones, R. M. (1975) *Mechanics of Composite Materials*. McGraw Hill.

Jørgensen, O. (1993) Ring-element analysis of layered orthotropic bodies. *Comp. Meth. Appl. Mech. Engng* **102,** 319–336.

Jørgensen, O. (1994a) Indentation failure in cross ply laminates, comparison between observations and 3-D field solutions. *J. Comp. Mat.* **28,** 1803–1824.

Jørgensen, O. (1994b) Delamination vs matrix cracking in layered composites subjected to transverse loading. *Eng. Frac. Mech.* **46**(6), 945–954.

Jørgensen, O. and Horsewell, A. (1997) On the indentation failure of carbon-epoxy cross-ply laminates, and its suppression by elasto-plastic interleaves. *Acta Mat.*, to appear.

Press, W., Teukolsky, B. and Vetterling, W. (1989) *Numerical Recipes*, pp. 390–400. Cambridge University Press.

Suresh, S., Giannakopoulos, A. E. and Alcala, J. (1997) Spherical indentation of compositionally graded materials. Theory and experiments. *Acta Mater.* **45,** 1307–1321.

Willis, J. R. (1996) Hertzian contact of anisotropic bodies. *Journal of the Mechanics and Physics of Solids* **14,** 163–176.